ISSN 1054-660X, Laser Physics, 2008, Vol. 18, No. 12, pp. 1530–1538.

Interaction/Laser Radiation with Matter Filamentation of Laser Pulses with Different Wavelengths in Air

V. Yu. Fedorov* and V. P. Kandidov

International Laser Center, Physics Department, Moscow State University, Moscow, 119992 Russia

e-mail: fedorov_v@mail.ru

Received July 7, 2008; in final form, July 10, 2008

Abstract—Propagation in the air of laser radiation with wavelengths in the range from 248 to 1240 nm are investigated numerically. It was shown that the intensity in a filament weakly depends on the wavelength in a long-wave region and decreases significantly in the UV region. Electron concentration in a plasma channel increases with a wavelength decrease with a dependence close to quadratic. With an increase in the wavelength characteristic scale of the intensity variation in the pulse cross section, the radii of the filament and plasma channel increase.

PACS numbers: 52.38.Hb, 42.65.Jx, 42.65.Tg, 33.80.Wz, 52.35.Mw

DOI: 10.1134/S1054660X08120232

INTRODUCTION

Lengthy filamentation of powerful femtosecond laser pulses in air was observed experimentally for the first time in [1–3]. The unique properties of the filamentation allow the use of this effect for the broadband LIDAR construction [4], lightning triggering or guiding [5], pulse compression [6, 7], as well as the remote laser-induced breakdown spectroscopy [8]. In most filamentation experiments, a Ti:sapphire laser with a 800-nm wavelength is used as the source of radiation. There are a series of papers, in which filaments in atmosphere air were observed using a 1060-nm wavelength radiation [9, 10] and radiation from the ultraviolet spectral region [11–16]. The main parameters of the filament and plasma channel obtained in these experiments are presented in the table. Comparing the results presented in this table, it is difficult to draw any conclusions about regularities in the variation of the filament and the plasma channel characteristics on the radiation wavelength.

Most theoretical papers until now have assumed that the wavelength of the laser pulse is equal to 800 nm (see, for example, [19, 20]). Theoretical investigations of the filamentation of laser pulses with a wavelength that differs from 800 nm, in general, support a particular experiment (for example, [11, 14]). The determination of the dependence of the filamentation parameters on the wavelength has not been the aim of these studies.

In the present paper, we numerically investigated the dependences of the filament and plasma channel characteristics during the filamentation of laser pulses with a variation in the wavelength in a wide range. For the determination of the spectral regularities of the femtosecond laser pulse filamentation, a unified model was built describing the air medium for a nonlinear optical response on the action of radiation with different wavelengths. Specific values of the wavelengths correspond to the existing sources of powerful femtosecond radiation. These include an 800-nm Ti:sapphire laser, a 400-nm second-harmonic Ti:sapphire [16], a 248-nm third-harmonic Ti:sapphire or the radiation of a dye laser [12], a 1060-nm Nd:glass laser [10], a 1240-nm Cr:forsterite laser [21], and a 600-nm second-harmonic Cr:forsterite.

SPECTRAL-DEPENDENT MODEL OF AIR FOR NONLINEAR OPTICAL RESPONSE

Powerful femtosecond laser pulse propagation in atmosphere is determined by nonlinear optical effects of Kerr self-focusing in air, defocusing in induced laser plasma, losses of energy due to air ionization, and linear wave processes of diffraction and dispersion. Investigating the effect of the wavelength on the filamentation process, we will take into account the dispersion dependence of the air medium parameters, determining the effects listed above.

Pulse self-focusing, which induces the birth of a filament, is determined by the nonlinear increment of a refractive index due to a high intensity. Self-focusing critical power $P_{cr}(\lambda)$ is determined by the following expression [22]:

$$P_{cr}(\lambda) = 3.77\frac{\lambda^2}{8\pi n_0 n_2(\lambda)}, \quad (1)$$

where n_0 is the linear refractive index and $n_2(\lambda)$ is the nonlinear coefficient of the air refractive index, which depends on the radiation wavelength. The values of the $n_2(\lambda)$ coefficient for several wavelengths were measured in [23–28]. The character of the cubic susceptibility dependence on wavelength λ were suggested in [29] on the basis of the experimental data processing in the

range from 480 to 700 nm. Using these data, we constructed the following approximation formula for the nonlinear coefficient of a refractive index on the wavelength for air at atmospheric pressure [30]:

$$n_2(\lambda) = 3 + \frac{6.37 \times 10^5}{\lambda^2}, \quad (2)$$

where the wavelength is in nanometers and $n_2(\lambda)$ units are 10^{-23} m^2/W. Using this formula for $\lambda = 800$ nm, coefficient $n_2(\lambda) = 4 \times 10^{-23}$ m^2/W; for $\lambda = 248$ nm, $n_2(\lambda) = 13.4 \times 10^{-23}$ m^2/W; and for $\lambda = 1240$ nm, $n_2(\lambda) = 3.4 \times 10^{-23}$ m^2/W.

Investigations of air filamentation were carried out, in general, for pulses at the $\lambda^{800} = 800$ nm wavelength, which can be considered the reference point during the analysis of the wavelength effect. Therefore, it is convenient to represent the self-focusing critical power $P_{cr}(\lambda)$ dependence on the wavelength in the form of the expansion near $P_{cr}(\lambda^{800})$:

$$P_{cr}(\lambda) = P_{cr}(\lambda^{800})(1 + 3.12 \times 10^{-3}\Delta\lambda + 2.36 \times 10^{-6}\Delta\lambda^2 - 1.82 \times 10^{-10}\Delta\lambda^3), \quad (3)$$

where $P_{cr}(\lambda^{800}) = 2.4$ GW is the critical power at the 800-nm wavelength, and the wavelength deviation $\Delta\lambda = (\lambda - \lambda^{800})$ is in nanometers. Figure 1 shows the dependence of critical power P_{cr} calculated using Eq. (3) and the values of P_{cr} presented in several papers. With an increase in the wavelength, the self-focusing critical power $P_{cr}(\lambda)$ grows and reaches $P_{cr} = 6.8$ GW for radiation with a 1240-nm wavelength, $P_{cr} = 2.4$ GW for 800 nm, and decreases to $P_{cr} = 0.07$ GW for a 248-nm wavelength. Thus, while the beam power is fixed, the Kerr self-focusing is more distinguished for pulses with a lower wavelength. One can see that the dispersion dependence of refractive index nonlinear coefficient (2) provides a small contribution, and the dependence of the self-focusing critical power on the wavelength is close to quadratic.

During the filamentation process, intensity growth due to Kerr self-focusing stops by defocusing in the generation of laser plasma, which causes the negative refractive index increment n_{pl}:

$$\Delta n_{pl} = -\frac{1}{2n_0}\frac{\omega_p^2}{\omega_0^2}, \quad (4)$$

where ω_0 is the central radiation frequency, $\omega_p = (e^2N_e/\varepsilon_0 m_e)^{1/2}$ is the plasma frequency depending on the free electron concentration N_e, ε_0 is the dielectric constant, e and m_e is the electron charge and mass, respectively.

The kinetic equation for the description of the variation of the free electron concentration N_e in a strong

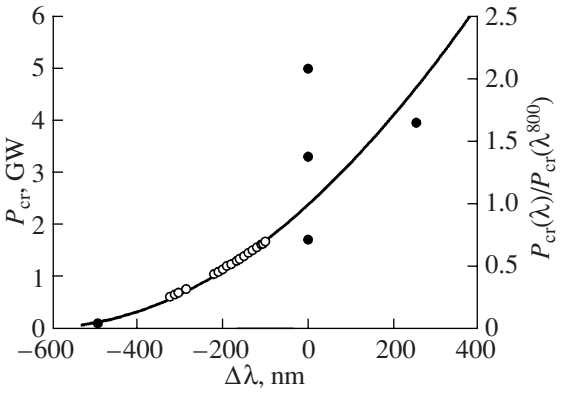

Fig. 1. Self-focusing critical power P_{cr} as a function of $\Delta\lambda = (\lambda - \lambda^{800})$. Curve—approximation dependence (3), full circles—experimental data [24–28], circles with hole—experimental data [29].

pulse laser field has the following form:

$$\frac{\partial N_e}{\partial t} = R(I, \lambda)(N_0 - N_e), \quad (5)$$

where I is the laser pulse intensity, $R(I, \lambda)$ is the ionization rate which depends on the intensity and radiation wavelength, and N_0 is the concentration of neutral molecules. Considering air as a mixture composed of nitrogen and oxygen, let us define the ionization rate for each component. According to the Keldysh theory [31], the character of the ionization process is determined using the parameter $\gamma = 2\pi c\sqrt{2m_eW_i}/\lambda eE$, where c is the light velocity, W_i is the ionization potential of the molecule, and E is the field strength of the electromagnetic wave. While $\gamma \gg 1$ ionization has a multiphoton character, $\gamma \ll 1$ shows a tunnel character. In the case of the multiphoton ionization, the dependence of the ionization rate on the intensity has the power law $R(I, \lambda) \sim I^{K(\lambda)}$, where the order of ionization process $K(\lambda)$ is determined by the expression

$$K(\lambda) = \mathrm{Int}\left[\frac{\lambda W_i}{2\pi\hbar c} + 1\right], \quad (6)$$

where the Int operation denotes the integer part of the value. Using its physical meaning, K is the number of field quanta of the laser pulse, which is necessary for the molecule ionization.

Figure 2 represents the dependence of parameter γ on the wavelength for molecules of nitrogen and oxygen in the case of a filament characteristic intensity equal to 10^{14} W/cm^2. One can see that, for UV radiation, the multiphoton ionization is dominating, whereas for IR radiation, the tunnel regime is predominant. Therefore, to describe the ionization of air gas components from the general point of view, it is necessary to use the general ionization model for the whole range of

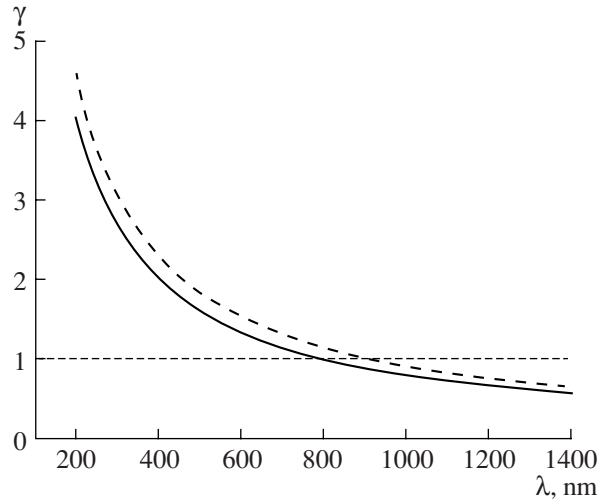

Fig. 2. Dependence of Keldysh parameter γ on the wavelength for oxygen (full curve) and nitrogen (dashed curve). The intensity is equal to 10^{14} W/cm^2.

wavelengths within our range of interest. In addition, it should include both the multiphoton and tunnel ionization regimes.

In our calculations, we consider air as a two-component medium, which consist of 20% oxygen molecules (W_i = 12.063 eV) and 80% nitrogen molecules (W_i = 15.576 eV). When the wavelength varies from 248 to 1240 nm, multiphoton order $K(\lambda)$ changes from 3 to 13 for oxygen molecules, and from 4 to 16 for nitrogen molecules.

Until now, the absolute values of the oxygen and nitrogen ionization rates as a function of the laser pulse intensity were determined experimentally for radiation with a 800-nm wavelength [32]. The closest fit of the experimental dependence yields the Perelomov–Popov–Terentiev (PPT) model [33]. The oxygen and nitrogen ionization rates, calculated using the PPT model for the observed wavelength and experimental data from [32] are presented in Fig. 3. One can see that the short-wave radiation ionization rate is significantly higher than for the long-wave rate at the same intensity. Moreover, for pulses with a 248- and 400-nm wavelength, ionization is significant at intensities which usually initially present in a laser pulse upon exiting the laser system. Thus, one may conclude that, in the case of short-wave radiation, free electrons of an induced

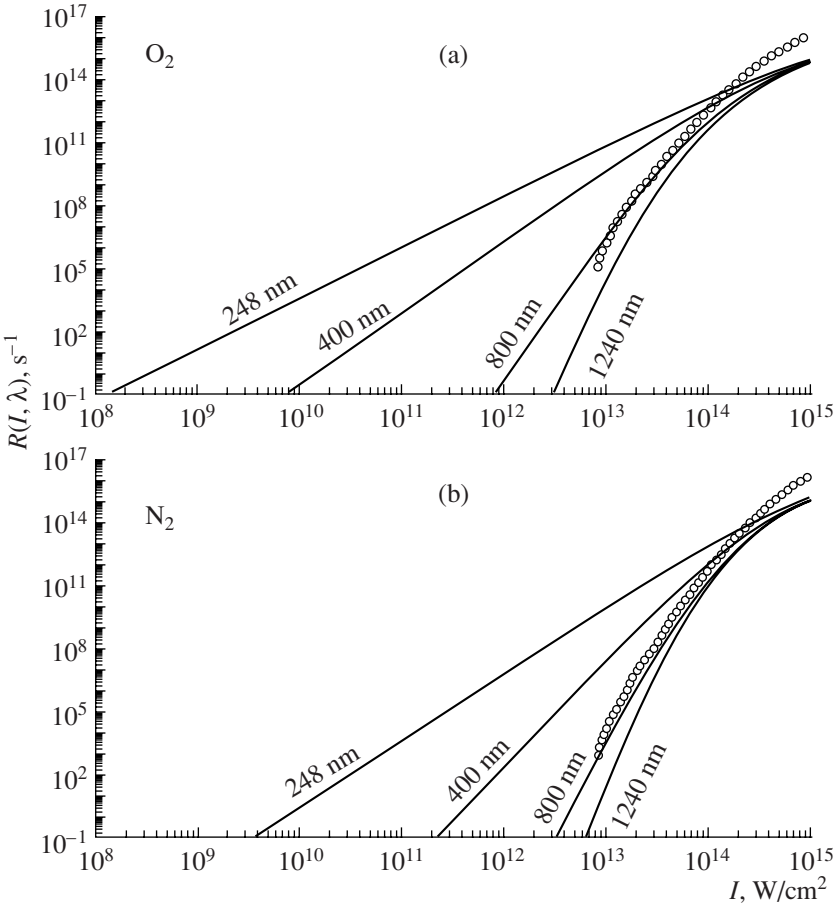

Fig. 3. Dependence of the PPT ionization rate on the intensity for several pulse wavelengths for oxygen (a) and nitrogen (b). Points—experimental data from [32].

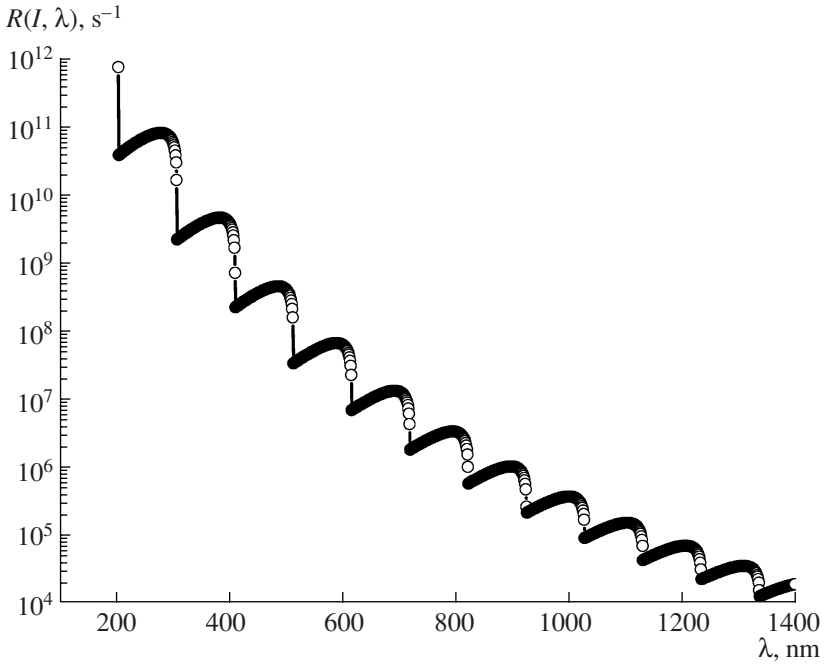

Fig. 4. Dependence of oxygen PPT ionization rate on wavelength. Intensity is equal to $I = 10^{12}$ W/cm^2. Wavelength difference between two points is equal to 1 nm.

laser plasma are generated before the pulse intensity increases by the Kerr self-focusing.

Note that, due to the discrete variation in the multiphoton order $K(\lambda)$ with the wavelength, ionization rate $R(I, \lambda)$ has a step function, while wavelength λ varies continuously (see Fig. 4). Thus, one can expect that there will be some features in the wavelength dependence of the filament and plasma channel parameters near wavelengths corresponding to a change in the multiphoton order of the ionization process.

The nonlinear absorption of radiation determined by the ionization of gaseous air components increases with a growth in this process probability. The absorption coefficient has the following form: $\alpha = I^{-1}K\hbar\omega_0\partial N_e/\partial t$, where I is the laser pulse intensity.

The dependences of the diffraction and dispersion wave effects on the wavelength are determined by the dependence of linear refractive index n_0 on the wavelength. The Cauchy formula is a good fit for the $n_0(\lambda)$ spectral dependence in atmospheric transparency windows [34]. Among the wavelengths we consider, only 248 nm lies beyond the atmospheric transparency window. However, for the laboratory experiments, where the filamentation takes place at short distances, linear absorption can be neglected.

In the slowly varying amplitude method approximation, the field complex amplitude variation of a high-power femtosecond laser pulse during its propagation in air is described by the following equation [35]:

$$2ik\frac{\partial E}{\partial z} = \Delta_\perp E - kk''_\omega\frac{\partial^2 E}{\partial t^2} + \frac{2k^2}{n_0}n_2|E|^2E - \frac{k^2}{n_0^2}\frac{\omega_p^2}{\omega_0^2}E - ik\alpha E, \quad (7)$$

where $k''_\omega = (\partial^2 k/\partial\omega^2)_{\omega=\omega_0}$. The first term on the right-hand side of Eq. (7) describes the diffraction, the second term describes the dispersion, the third term describes the Kerr nonlinearity, the fourth term describes the nonlinearity due to induced laser plasma, and the fifth terms describes the energy absorption in the ionization process.

RESULTS OF COMPUTER SIMULATIONS AND THEIR ANALYSIS

Investigating the filamentation in the air of laser radiation with different wavelengths, we considered transform-limited pulses with a Gaussian shape and a Gaussian intensity distribution in the cross section:

$$E(r, t, z = 0) = E_0\exp\left(-\frac{r^2}{2a_0^2}\right)\exp\left(-\frac{t^2}{2\tau_0^2}\right). \quad (8)$$

Table 1. Filament and plasma channel parameters obtained in the experiment: I_{fil}—intensity in filament, N_e^{fil}—free electron concentrations in the plasma channel, d_{fil}—filament diameter, d_{pl}—plasma channel diameter

λ, nm	I_{fil}, W/cm^2	N_e^{fil}, 10^{16} cm^{-3}	d_{fil}, μm	d_{pl}, μm	Source
248	10^{12}	3×10^{15}–10^{16}	100–150	–	[11, 12, 14]
406	–	–	100	–	[16]
527	6×10^{12}	–	120	–	[15]
800	5×10^{13}–10^{14}	10^{16}–10^{17}	80–150	50–65	[1, 2, 17, 18]
1053	5×10^{12}	10^{16}	100–1000	–	[9]

Table 2. Filament and plasma channel parameters obtained in the simulation: P/P_{cr}—number of critical powers in the initial beam, z_{fil}—filament start distance, I_{fil}—intensity in the filament, N_e^{fil}—free electron concentrations in the plasma channel, r_{fil}—filament radius, r_{pl}—plasma channel radius. The initial pulse parameters are energy W = 8 mJ, full length at e^{-1} τ_0 = 200 fs, beam radius a_0 = 1.2 mm, and intensity $I_0 = 10^{12}$ W/cm^2

λ, nm	P/P_{cr}	z_{fil}, m	I_{fil}, 10^{13} W/cm^2	N_e^{fil}, 10^{16} cm^{-3}	r_{fil}, μm	r_{pl}, μm
248	163.95	1.52	1.13	10.89	71.3	14.54
400	32.95	1.69	4.83	9.66	66.09	19.03
600	10.01	2.34	5.93	3.54	88.52	26.16
800	4.72	3.04	6.54	1.73	112.38	32.69
1060	2.44	4.23	6.66	0.82	145.44	39.63
1240	1.68	5.79	6.49	0.48	171.69	45.02

In pulses with different wavelengths, energy W, duration τ_0, and beam radius a_0 were the same; therefore, peak intensity I_0 was also the same. For the numerical simulation of system (5), (7), and (8), the numerical scheme [36] with a nonuniform grid in radial coordinate r and time coordinate t were used. Also, the adaptive integration step over longitudinal coordinate z was used.

Table 2 represents the filament and plasma channel parameters, obtained using the numerical simulation of the propagation of pulses with the following parameters: W = 8 mJ, τ_0 = 100 fs, a_0 = 1.2 mm, and $I_0 = 10^{12}$ W/cm^2. All of the parameters of filament and plasma channel shown in the tabled were determined at distance z_{fil}, where the intensity in the central pulse time layer was saturated. This distance was treated as the filament starting point. There is a ratio of peak power P for a pulse with a different wavelength to self-focusing critical power P_{cr} as shown in the table. While the pulse peak power is fixed, the P/P_{cr} ratio varies within two orders for the wavelength range under consideration. It decreases during the shift to the long-wave region. Thus, with an increase in the laser pulse wavelength, the filament start distance increases in spite of the diffraction length ka_0^2 increase. The derived result corresponds to the dependence described by the Marburger formula [22]:

$$z_{\text{fil}} = \frac{0.367ka_0^2}{\left\{\left[\left(\frac{P}{P_{\text{cr}}(\lambda)}\right)^{1/2} - 0.852\right]^2 - 0.0219\right\}^{1/2}}. \quad (9)$$

The values of intensity in the filament for the observed wavelengths are presented in Fig. 5. In this figure, the points corresponding to the radiation of the existing femtosecond laser sources are represented. In addition, in Fig. 5, the I_{fil} values correspond to the wavelengths, which determine the boundaries of the spectral ranges with the same multiphoton order $K(\lambda)$ are shown. For clarity, the values $K(\lambda)$ which are the same are connected by segments. One can see that the filament intensity dependence on the wavelength has a nonmonotonic character. This can be explained, as mentioned before, by stepwise changes in the ionization probability during the multiphoton order change. Note that while, multiphoton order $K(\lambda)$ increases with an increase in the wavelength, the ionization probability jumps decrease. This leads to a more monotonic dependence for the filament intensity on the wavelength. In general, the intensity of filament I_{fil} is weakly dependent on the wavelength in the long-wave spectral region and significantly decreases in the UV spectral region.

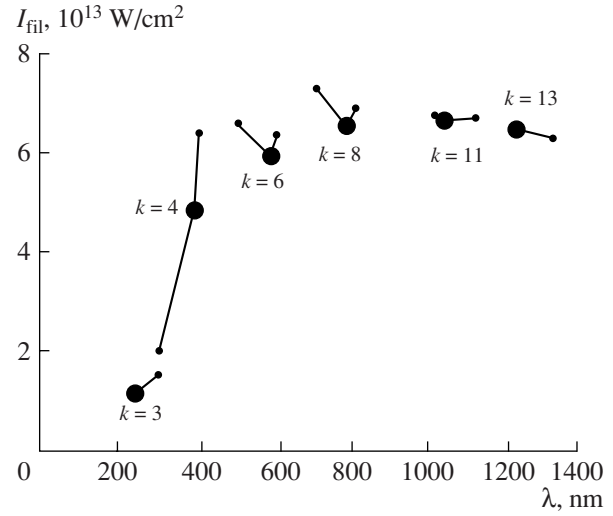

Fig. 5. Dependence of the intensity in the filament on the pulse wavelength. Big points—numerical simulation for wavelengths corresponding to existing laser sources; small points—numerical simulation for wavelengths which correspond to the borders of spectral regions with the same multiphoton order $K(\lambda)$ of oxygen.

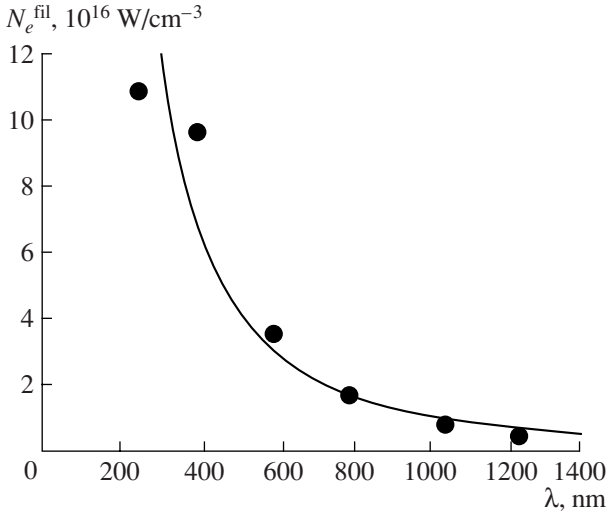

Fig. 6. Free electron concentrations in the plasma channel as a formula of the pulse wavelength. Points—numerical simulation, curve—formula (12).

Thus, for pulses in he spectral range 600–1240 nm, the intensity can be treated as wavelength independent.

For the qualitative analysis of the filament and plasma channel parameters, the dependence on the wavelength assumes that near the filament start distance, the absolute values of the refractive index increments due to the Kerr effect and defocusing in the laser plasma become equal:

$$n_2 I(z_{fil}) = \frac{\omega_p^2}{2n_0\omega_0^2}. \quad (10)$$

Such an approach was used in [37] for the I_{fil} estimation in a pulse with a 800-nm wavelength. Denoting the electron concentration of induced laser plasma at the filament start distance as N_e^{fil}, equality (10) can be written as

$$n_2(\lambda) I_{fil} \sim \lambda^2 N_e^{fil}. \quad (11)$$

As follows from the numerical analysis of pulses from the long-wave spectral region (600—1240 nm), the intensity in filament I_{fil} can be considered as constant.

While the wavelength varies in the long-range spectrum region, the variation in the refractive index nonlinear coefficient n_2 is less than 1.4 and, for simplicity, it can be considered as constant. Then, from expression (11), it follows that the electron concentration in the plasma channel is inversely proportional to the square of the wavelength (Fig. 6)

$$N_e^{fil} \sim \frac{1}{\lambda^2}. \quad (12)$$

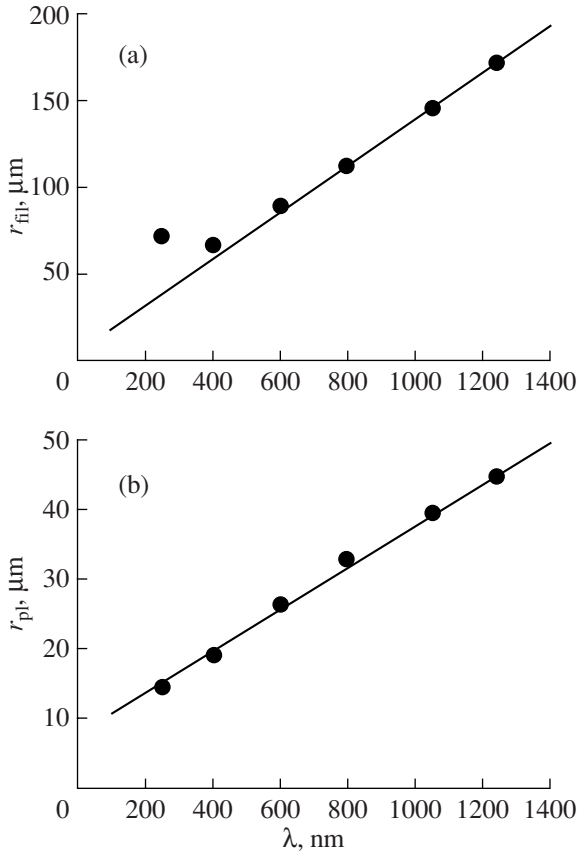

Fig. 7. Dependence of the filament radius (a) and plasma channel radius (b) on the wavelength. Points—numerical simulation, curve—formula (13).

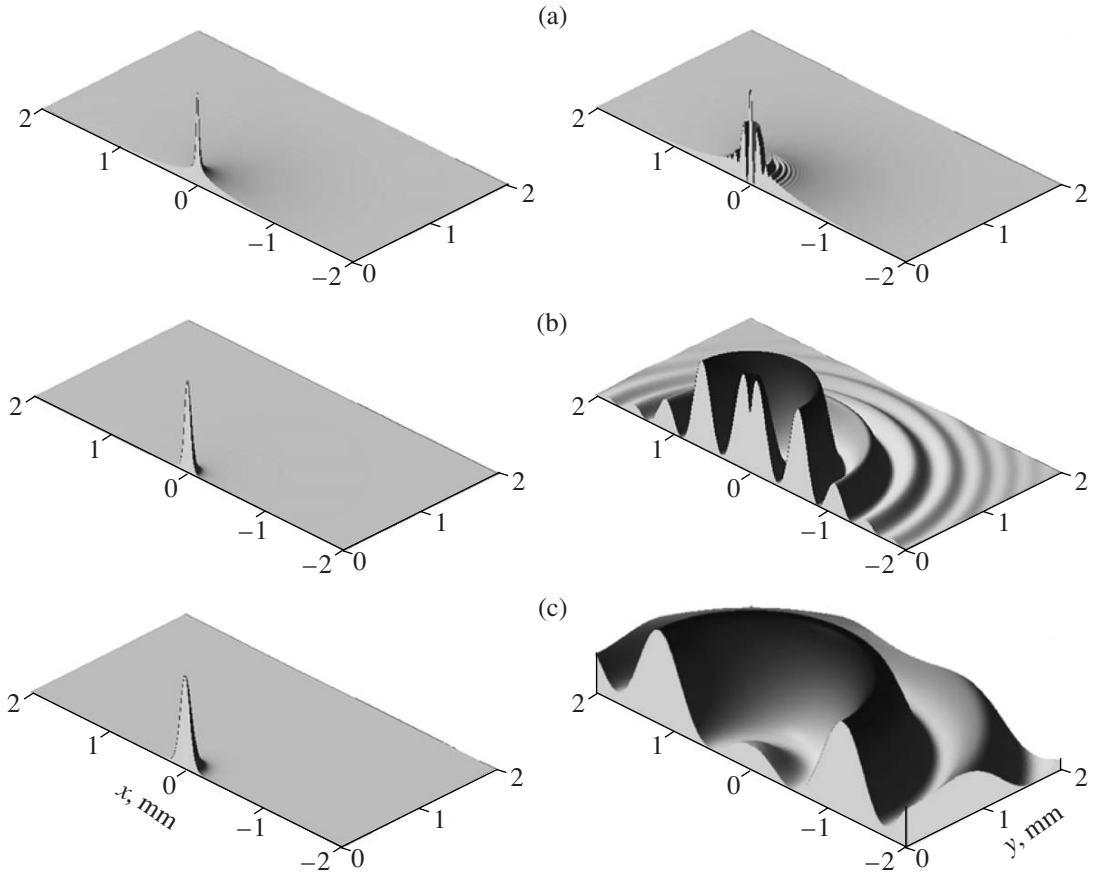

Fig. 8. Intensity distribution in the central pulse time layer on two characteristic distances: left—at the filament start distance, right—at the distance of the initial refocusing. (a) Pulse at 248 nm, (b) at 800 nm, and (c) at 1240 nm. The parameters of the pulses are as follows: 8 mJ energy, 200 fs duration (e^{-1}), 1.2 mm radius, and 10^{12} W/cm^2 intensity.

The electron concentration values N_e^{fil} obtained in the numerical simulation are close to dependence (12), especially in the long-wave range.

The values for filament radius r_{fil}, listed in Table 2, show that r_{fil} increases with an increase in the wavelength. For the estimation, we assume that the filament contains power about critical power $P_{\text{cr}} \sim \pi r_{\text{fil}}^2 I_{\text{fil}}$. Taking into account the expression for self-focusing critical power (1) with I_{fil} = const, we find that the filament radius is proportional to wavelength λ:

$$r_{\text{fil}}(\lambda) \sim \lambda. \tag{13}$$

Figure 7a shows the filament radius r_{fil} for dependence (13) on wavelength λ. In addition, the numerical simulation data is shown here. Analytical dependence (13) of filament radius r_{fil} on wavelength λ qualitatively matches the results of the numerical simulation.

We also show that the linear dependence on the wavelength is also valid for plasma channel radius r_{pl} (Fig. 7b):

$$r_{\text{pl}} \sim \lambda. \tag{14}$$

The radiation wavelength has a significant influence on radial intensity I and energy density J distribution in the filament cross section. In Fig. 8, for several wavelengths are shown for the intensity distributions in the central time slice for the pulse on two characteristic distances: at the filament start distance and at the first refocusing point, where at the initial time intensity in the central pulse layer begins increasing again.

From this picture, one can see that, in the pulse cross section, with an increase in the wavelength, a characteristic scale with a ring-type structure, which formed due to the defocusing in the induced laser plasma, increases. Thus, for a pulse with a 248-nm wavelength, the interval between two neighbor rings d equals 80 μm, for a 800-nm wavelength, d = 480 μm, while for 1240 nm, d = 900 μm. We assume that the ring structure in the intensity distribution is an effect of the interference of two waves: conical wave running from the beam center (its nature is defocusing in the laser plasma) and the background plane wave [38]. Then, we can estimate period d of a formed interfer-

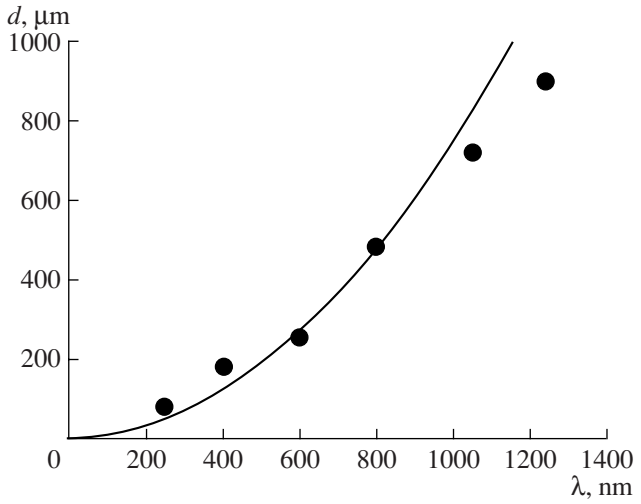

Fig. 9. Dependence of the interference ring periods on the wavelength. Points—numerical simulation, curve—formula (15).

ence structure using formula

$$d \sim \frac{\lambda}{\theta(\lambda)}. \quad (15)$$

The divergence angle of the conical wave defocusing in plasma can be taken proportional to $\Delta n_{pl}/r_{pl}$. In accordance with Eq. (10), $\Delta n_{pl} \sim n_2(\lambda)I_{fil}(\lambda)$, which, as follows from Table 2, varies no more than 25% in the spectral region under consideration. This implies that, for the conical wave divergence angle, the following estimation is valid:

$$\theta(\lambda) \sim \frac{1}{r_{pl}(\lambda)} \sim \frac{1}{\lambda}. \quad (16)$$

Thus, for the period of the interference rings, we finally obtain

$$d \sim \lambda^2. \quad (17)$$

Figure 9 shows dependence (17) and the numerical simulation results.

We performed a similar analysis for pulses with a different energy, beam radius, and intensity. We considered energies from 0.2 to 24.0 mJ, beam radiuses from 0.2 to 2.0 mm, and initial intensities from 0.2×10^{12} to 1.7×10^{13} W/cm^2. The estimations we carried out above remain valid for a wide range of the initial pulse parameters and qualitatively describe the filament and plasma channel parameter variations with a variation of a laser pulse wavelength.

CONCLUSIONS

We carried out a numerical simulation of the filamentation of powerful femtosecond laser pulses with different wavelengths and determined the characteristics of the filament and plasma channel. With a decrease in λ, the filament and plasma channel radius decreases; the electron concentration in the laser plasma increases. The intensity variation in the filament does not exceed 10% for wavelengths from 1240 to 600 nm and decreases in the ultraviolet region.

Simulations were completed on the basis of a general model of the nonlinear-optic response of gaseous air components on the action of powerful femtosecond laser pulses with different wavelengths. On the basis of the generalization of experimental and theoretical results, we obtained empirical formula for the cubic air nonlinear coefficient dependence on λ.

ACKNOWLEDGMENTS

This work was partially funded by the Russian Foundation for Basic Research (project nos. 06-02-08004 and 08-02-00517-a).

REFERENCES

1. A. Braun, G. Korn, X. Liu, et al., Opt. Lett. **20**, 73 (1995).
2. E. T. J. Nibbering, P. F. Curley, G. Grillon, et al., Opt. Lett. **21**, 62 (1996).
3. A. Brodeur, C. Y. Chien, F. A. Ilkov, et al., Opt. Lett. **22**, 304 (1997).
4. J. Kasparian, M. Rodriguez, G. Mejean, et al., Science **301**, 61 (2003).
5. X. M. Zhao, J.-C. Diels, C. Y. Wang, and J. M. Elizondo, IEEE J. Quantum Electron. **31**, 599 (1995).
6. O. G. Kosareva, I. N. Murtazin, N. A. Panov, et al., Laser Phys. Lett. **4**, 126 (2007).
7. J. Liu, X. W. Chen, R. X. Li, and T. Kobayashi, Laser Phys. Lett. **5**, 45 (2007).
8. P. Rohwetter, K. Stelmaszczyk, L. Woste, et al., Spectrochim. Acta B **60**, 1025 (2005).
9. B. La Fontaine, F. Vidal, Z. Jiang, et al., Phys. Plasmas **6**, 1615 (1999).
10. P. Béjot, L. Bonacina, J. Extermann, et al., Appl. Phys. Lett. **90**, 151106 (2007).
11. J. Schwarz, P. Rambo, J.-C. Diels, et al., Opt. Commun. **180**, 383 (2000).
12. S. Tzortzakis, B. Lamouroux, A. Chiron, et al., Opt. Lett. **25**, 1270 (2000).
13. T. R. Nelson, T. S. Luk, A. C. Bernstein, and S. Cameron, "Laser Filamentation of a Femtosecond Pulse in Air at 400 nm," *Proceedings of the QELS'01, Baltimore, USA, 2001*, p. 261
14. S. Tzortzakis, B. Lamouroux, A. Chiron, et al., Opt. Commun. **197**, 131 (2001).
15. D. Mikalauskas, A. Dubietis, and R. Danielus, Appl. Phys. B **75**, 899 (2002).
16. B. Prade, M. Franco, A. Mysyrowicz, et al., Opt. Lett. **31**, 2601 (2006).
17. S. Tzortzakis, B. Prade, M. Franco, and A. Mysyrowicz, Opt. Commun. **181**, 123 (2000).

18. J. Liu, Z. Duan, Z. Zeng, et al., Phys. Rev. E **72**, 026412 (2005).
19. O. G. Kosareva, V. P. Kandidov, A. Brodeur, and S. L. Chin, J. Nonlinear Opt. Phys. Mater. **6**, 485 (1997).
20. M. Mlejnek, E. M. Wright, and J. V. Moloney, Opt. Lett. **23**, 382 (1998).
21. M. B. Agranat, S. I. Ashitkov, A. A. Ivanov, et al., Quantum Electron. **34**, 506 (2004).
22. J. H. Marburger, Prog. Quantum Electron. **4**, 35 (1975).
23. M. J. Shaw, and C. J. Hooker, Opt. Commun. **103**, 153 (1993).
24. Y. Shimoji, A. T. Fay, R. S. F. Chang, and N. Djeu, J. Opt. Soc. Am. B **6**, 1994 (1989).
25. R. W. Hellwarth, D. M. Pennington, and M. A. Henesian, Phys. Rev. A **41**, 2766 (1990).
26. E. T. J. Nibbering, G. Grillon, M. A. Franco, et al., J. Opt. Soc. Am. B **14**, 650 (1997).
27. W. Liu and S. L. Chin, Opt. Express **13**, 5750 (2005).
28. D. M. Pennington, M. A. Henesian, and R. W. Hellwarth, Phys. Rev. A **39**, 3003 (1989).
29. V. Mizrahi and D. P. Shelton, Phys. Rev. Lett. **55**, 696 (1985).
30. V. Y. Fedorov and V. P. Kandidov, Opt. Spectrosc. **105**, 291 (2008).
31. L. V. Keldysh, Sov. Phys. JETP **20**, 1307 (1965).
32. A. Talebpour, J. Yang, and S. L. Chin, Opt. Commun. **163**, 29 (1999).
33. A. M. Perelomov, V. S. Popov, and M. V. Terent'ev, Sov. Phys. JETP **23**, 924 (1966).
34. D. R. Lide, *CRC Handbook of Chemistry and Physics, Internet Version 2007* (Taylor and Francis, Boca Raton, FL, 2007).
35. O. G. Kosareva, V. P. Kandidov, A. Brodeur, et al., Opt. Lett. **22**, 1332 (1997).
36. V. P. Kandidov and V. Y. Fedorov, Quantum Electron. **34**, 1163 (2004).
37. J. Kasparian, R. Sauerbrey, and S. L. Chin, Appl. Phys. B **71**, 877 (2000).
38. S. L. Chin, S. Petit, W. Liu, et al., Opt. Commun. **210**, 329 (2002).